Enhanced Expansion and Reduced Kiss-and-Run Events in Fusion Pores Steered by Synaptotagmin-1 C2B Domains

Ary Lautaro Di Bartolo,[†,‡] Claudia N. Tomes,[†,‡] Luis S. Mayorga,[†,‡] and Diego Masone[*,†,¶]

†*Instituto de Histología y Embriología de Mendoza (IHEM) - Consejo Nacional de Investigaciones Científicas y Técnicas (CONICET), Universidad Nacional de Cuyo (UNCuyo), 5500, Mendoza, Argentina*

‡*Facultad de Ciencias Exactas y Naturales, Universidad Nacional de Cuyo (UNCuyo), 5500, Mendoza, Argentina*

¶*Facultad de Ingeniería, Universidad Nacional de Cuyo (UNCuyo), 5500, Mendoza, Argentina*

E-mail: diego.masone@ingenieria.uncuyo.edu.ar

Phone: +54 261 405 4843

Abstract

The fusion pore controls the release of exocytotic vesicles contents through a precise orchestration of lipids from the fusing membranes and proteins. There is a major lipid reorganization during the different stages in life of the fusion pore: membrane fusion, nucleation and expansion, that can be scrutinized thermodynamically. In this work, using umbrella sampling simulations we describe the expansion of the fusion pore. We have calculated free energy profiles to drive a nascent, just nucleated, fusion pore to its expanded configuration. We have quantified the effects on the free energy of one and two Synaptotagmin-1 C2B domains in the cytosolic space. We show that C2B domains cumulatively reduce the cost for expansion, favoring the system to evolve towards full fusion. Finally, by conducting thousands of unbiased molecular dynamics simulations, we show that C2B domains significantly decrease the probability of kiss-and-run events.

Introduction

Exocytosis is a key mechanism used by eukaryotic cells to release biological compounds and to transport molecules across the plasma membrane. As a response to physiological signals, specialized secretory cells undergo regulated exocytosis.[1] In particular, sperm exocytosis (or acrosome reaction) is a regulated secretion required to fertilize the egg that depends on large bilayer remodeling, such as membrane bending and fusion.[2–4] During this unique process, multiple fusion pores form between the acrosomal and plasma membranes, connecting the lumen of the acrosome to the extracellular milieu.[5–7] Accurate molecular mechanisms that describe membrane fusion and the formation of the fusion pore have been objects of research among the experimental[8,9] and computational[10–13] sciences.

After membrane fusion, the nucleation of a nascent fusion pore (which in thermodynamic terms is the first step in the formation of a new configuration) can follow different possible paths: dilation (meta-stabilization), transient flickering (open-close repetitions) or

kiss-and-run resealing (the metastable pore closes and bilayers evolve towards full recovery).[14] Therefore, the complete free energy landscape along the different stages of the fusion pore becomes a desirable description to quantitatively determine the position of local minima that could restrain the fusion pore from evolving in either one of these paths.

As broadly reported in the literature, the free energy cost to induce a trans-membrane pore in a single lipid bilayer is highly dependent on its lipid composition.[15,16] For membrane fusion, energetics are not only determined by the lipid composition[17] but also by the hydration level of the bilayers for different inter-membrane distances.[8,18,19] These effects can be extrapolated to the more complex fusion pore configuration, combining membrane fusion and a water channel formation. Therefore, it is expected that the free energy to form a fusion pore highly depends on the membranes molecular compositions and their inter-membrane separation.[16,19–21]

Using a stalk-guided fusion pore and continuum model simulations with the SDK force-field[22] for opposed bilayers at 6.1nm (center-to-center distance), Kawamoto and Shinoda[21,23] calculated the free energy cost to nucleate a fusion pore between bilayers, with the following results: $\sim$100 k_BT for DOPC:DOPE (1:1), $\sim$120 k_BT for DMPC:DOPE (1:1), $\sim$200 k_BT for DMPC:DOPC (1:1) and $\sim$250 k_BT for pure DMPC. In good agreement, using Gromacs and the Martini 2 coarse-grained model, we have previously reported $\sim$160 k_BT ($\sim$400 kJ/mol) for pure DPPC bilayers and $\sim$140 k_BT ($\sim$350 kJ/mol) for POPC:POPS:POP2 (87.5:10:2.5).[24] Comparatively, the cost to drive a just nucleated fusion pore into a metastable (slightly expanded) configuration is significantly lower. Again, Kawamoto and Shinoda[21,23] reported $\sim$30 k_BT to stabilize a nucleated fusion pore for DOPC:DOPE (1:1), $\sim$20 k_BT for DMPC:DOPE (1:1), almost no difference for DMPC:DOPC (1:1) and an energy increase of $\sim$10 k_BT for pure DMPC.

Recently, Hub and collaborators have developed a set of two reaction coordinates to respectively induce[25] and expand[26] a transmembrane hydrophilic pore in a single lipid bilayer. Here, we have generalized the latter methodology to expand a toroid-shaped fusion pore,

formed by two independent bilayers (Prof. Hub generously shared with us his source code through personal communication). Through umbrella sampling simulations, we have quantified the effects of Synaptotagmin-1 (Syt1) C2B domains (PDB ID:1K5W[27]) on the free energy landscape during the expansion of the fusion pore. We have observed that the effects are cumulative: one and two C2B domains progressively lower the free energy needed to expand the metastable fusion pore. Remarkably, C2B domains boost just nucleated, nascent fusion pores in the direction of expansion, though reducing the probability of kiss-and-run events.

Together with our previous studies on membrane fusion and pore nucleation,[24,28] we complete here another step along the life of the fusion pore by describing its expansion. We have ported the nucleation and expansion processes into two convenient collective variables for the PLUMED 2 development version environment (https://github.com/plumed/plumed2),[29] easily compilable as an optional module and with source codes freely available on GitHub: https://github.com/lautarodibartolo/FusionPore. The expansion procedure can be directly used for free energy calculations with any pair of homogeneous/heterogeneous lipid bilayers, at different hydration levels, with or without proteins under the Martini 3 coarse-grained model.[30]

Results and discussion

Following the membrane composition used by Jahn and collaborators[31] to trap Syt1 to the plasma membrane in the presence of calcium, along this work we have used a pair of 1024 lipid bilayers under the new Martini 3 coarse-grained model,[30] containing 87.5% of 1-palmitoyl-2-oleoyl-glycero-3-phosphocholine (POPC), 10% of 1-palmitoyl-2-oleoyl-sn-glycero-3-phospho-L-serine (POPS) and 2.5% of the recently developed phosphatidylinositol 4,5-bisphosphate (PI(4,5)P_2, or simply PIP_2) model.[32] We have set the inter-membrane distance to ∼3.9nm (measured between opposed PO4 head group planes of different bilayers) which effortlessly

fits a Syt1-C2B domain able to interact with both cytosolic leaflets simultaneously.

As reported in the literature, the C2B polybasic region KRLKKKKTTIKK (positions 321-332)[33,34] and the arginine pair (R398,R399)[35] are key during large membrane remodeling processes mediated by Syt1, such as fusion and pore expansion. In particular, the polybasic patch in C2B binds to negatively charged lipids, such as PIP_2 clusters, in a calcium-independent manner.[36–40] Although in the atomistic space the inclusion of Ca^{2+} ions to model the penetration depth of the C2B binding loop would be in principle the right approach, with coarse-grained models the strategy is not straightforward. In the reduced resolution space, the parameterization of metal ions is still approximated or unavailable for the most of coarse-grained force fields.[41] For Martini, ions are modeled with single beads representing both the ion itself and the first hydration shell.[42] Therefore, in this work we have described Syt1-C2B binding mechanisms in a calcium-independent manner.

Based on an event-oriented classification for the different stages of the fusion pore[18,23,43–45] and in resemblance with the biological process of a vesicle about to fuse with the plasma membrane, as schematically shown in figs. 1a and 1b, we have used independent collective variables for membrane fusion (ξ_f),[28] fusion pore nucleation (ξ_n) and expansion (ξ_e), see eqs. 1, 2 and 3. From initially flat and parallel opposed POPC:POPS:PIP_2 bilayers, using restrained molecular dynamics simulations we have sequentially induced the fusion stalk (figure 1c), a traversing water channel through it (figure 1d) and its final expansion (figure 1e).

Membrane fusion, fusion pore nucleation and fusion pore expansion: ξ_f, ξ_n and ξ_e

The collective variables nomenclature follows the same formulation originally developed by Hub and collaborators[19,25,26] and our previous works in membrane fusion[28] and fusion pore nucleation.[24] Conceptually, ξ_f and ξ_n are analogous (see eqs. 1 and 2). Each one defines a cylinder of radius R_{cyl} with N_s slices of thickness d_s that can be filled by any user-defined

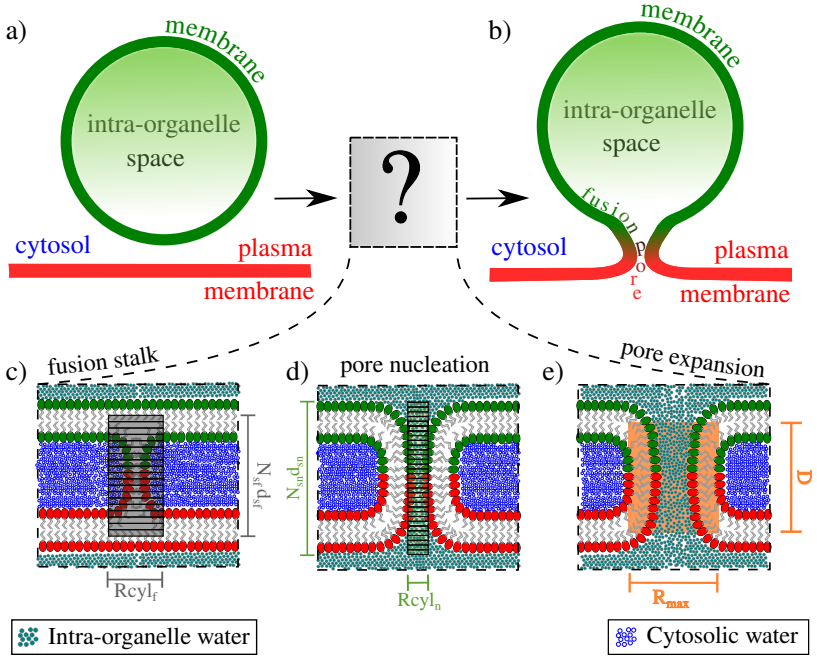

Figure 1: **Three stages in the life of the fusion pore. a)** Representation of a vesicle separated from the plasma membrane. **b)** Vesicle connected with the plasma membrane through a fusion pore. **c)** Spanning cylinder that defines collective variable ξ_f to fuse hemi-layers (gray). **d)** Cylinder connecting the intra-organelle space with the extra-cellular milieu that defines ξ_n and nucleates the fusion pore (green). **e)** Expansion of the fusion pore with collective variable ξ_e using the single-slice cylinder (orange).

bead types according to an occupation factor ζ (the fraction to which a slice is filled upon the addition of the first atom in the slice). Figure 1 shows a schematic representation of the fusion pore between a vesicle and the plasma membrane, together with the geometrical definition for collective variables ξ_f, ξ_n and ξ_e.

Recently, we have used eq. 1 to fuse membranes inducing a fusion stalk.[28] Here, starting from the fusion stalk we have sequentially used eq. 2 for fusion pore nucleation and eq. 3 for its expansion.

$$\xi_f = \frac{1}{N_{sf}} \sum_{s=0}^{N_{sf}-1} \delta_{sf}({N_{sf}}^{(p)}) \tag{1}$$

$$\xi_n = \frac{1}{N_{sn}} \sum_{s=0}^{N_{sn}-1} \delta_{sn}({N_{sn}}^{(q)}) \tag{2}$$

$$\xi_e = \frac{R(r) - R_0}{R_0} \tag{3}$$

In eq. 1, membrane fusion is induced using a spanning cylinder composed of N_{sf} slices (see fig. 1c). ${N_{sf}}^{(p)}$ accounts for the number of tail beads (C4A, C4B or C5A) within slice s inside the fusion cylinder. δ_{sf} is a continuous function in the interval [0 1] (δ_{sf}=0 for no beads in slice s and δ_{sf}=1 for 1 or more beads in slice s). In eq. 2, fusion pore nucleation is achieved with a different cylinder (composed of N_{sn} slices, see fig. 1d) now applied to an also different group, containing lipid heads (PO4), dynamically defined intra-organelle (W) water beads and accounted by ${N_{sn}}^{(q)}$. For the rest, ξ_n is analogous to ξ_f. For mathematical details see the original article.[25]

Eq. 3 is a normalized radius (by the simulation dependent parameter R_0) of the first approximation to the expanded fusion pore radius $R(r) = \sqrt{\frac{n_p(r)v0}{\pi D}}$. This radius is calculated dynamically at each simulation step using the number of intra-organelle water beads $n_p(r)$ inside a horizontal layer (parallel to the membranes) of height D, placed at the local Z center (Z_l) of all lipids inside a cylinder of radius R_{max} around the nucleated fusion pore (see figure 1e). $R(r)$ is then the radius of a cylinder of volume $\pi D R(r)^2$ which, when normalized by the volume of one W Martini bead[30] ($v0 = 0.076879nm^3$), equals the amount of water molecules inside the fusion pore $n_p(r)$.

Generalization to the fusion pore

As proposed before, lipid tails beads are a convenient group to induce membrane fusion.[19,24] By pulling from tail beads, lipids are tilted and reorganized to fuse radially displacing cytosolic waters. This pulling mechanism splays the nearest lipids towards the fusion patch, inducing a hydrophobic core. Therefore, for POPC and POPS lipids, collective variable ξ_f pulls from C4A and C4B tail beads, while for PIP_2 it pulls from C4B and C5A tail beads (see supporting information for beads labels). Subsequently, for fusion pore nucleation, collective

variable ξ_n pulls from intra-organelle water beads (W) and lipid phosphate heads (PO4). Finally, for fusion pore expansion ξ_e makes the water channel to widen and the fusion pore to expand by radially pulling from intra-organelle water beads (W) and lipid phosphate heads (PO4). However, the generalization of eq. 3 for the fusion pore from its original purpose to expand a hydrophilic pore in a single bilayer,[26] required the following modifications:

a) Interactive water molecules

Clearly defined intra-organelle and cytosolic spaces are inherent to the biological concept of the fusion pore (figs. 1a and 1b). Therefore, mutually exclusive groups of intra-organelle and cytosolic water beads becomes a convenient definition for our simulation systems (figs. 1c to 1e). Then, collective variable ξ_e dynamically selects at each molecular dynamics step if a water bead is intra-organelle or cytosolic. Specifically, a water molecule belongs to the intra-organelle subgroup if it fulfills 1 out of the following 3 conditions: (i) W is above the Z plane that contains the geometric center of the upper bilayer, or (ii) W is below the Z plane that contains the geometric center of the lower bilayer, or (iii) W is inside the cylinder of radius R_{max} that defines expansion. Any W bead not belonging to the intra-organelle subgroup is considered cytosolic. This is not only an improvement in terms of computational performance but also, it avoids possible errors due to water beads permeating through the bilayers from the intra-organelle space into the cytosol and vice-versa (especially for very long μs-length simulations).

b) Membrane undulations

1024 lipid bilayers are relatively large and naturally exhibit undulations that render the Z center between both membranes inadequate for calculations.[26] Instead, we have used here the local center Z_l of the cylindrical volume of height D and radius R_{max} where the water channel locally forms in the XY plane (see figure 1e). The position of this cylindrical volume is dynamically calculated at each molecular dynamics step, always centered around the water

channel. In this way, large membrane undulations have negligible effects on the Z_l position now taken as reference by ξ_e for the dynamic location of the horizontal layer (parallel to the membranes) of radius R_{max} and height D.

c) Toroid-shaped fusion pore

We have used the amount of water molecules inside the cylinder that expands the fusion pore to directly estimate its radius (see figure 1e). Martini W beads randomly accommodate in the available space in the most compact way, which results in a maximum density of ∼63.33 per cent (see supplementary information). Theoretically, the most compact way to pack spheres (random close packing) results in a maximum density of ∼64 per cent.[46–48] Following a statistical description of jammed states, Makse and collaborators[49] showed that random packing of hard spheres in three dimensions cannot exceed a density limit of ∼63.4 per cent. This last result is in excellent agreement with the behavior of Martini beads under unbiased conditions in an NPT equilibrated water box (see supporting information). Therefore, in the Martini space, any volume V occupied by N water beads is the sum of all the individual volumes $\sum_1^N v_i$ divided by the 0.634 random packing correction, $V = \frac{1}{0.634}\sum_1^N v_i$.

Given the scheme of a cylindrical torus as in figure 2a with internal radius r and external radius R, its volume is calculated by eq. 4. There, the volume of the torus is decomposed in the sum of its inner and outer halves (V_{inner} and V_{outer}), generated by rotating two half-discs of radius r, areas $\frac{\pi r^2}{2}$ and with centroids $r_c = \frac{4}{3\pi}r$, respectively along lengths $2\pi(R \pm r_c)$. For more details, see supporting information.

$$V_{toroid} = V_{inner} + V_{outer} = R\pi^2 r^2 - \frac{4}{3}\pi r^3 + R\pi^2 r^2 + \frac{4}{3}\pi r^3 = 2\pi R\pi r^2 \tag{4}$$

Given also a cylinder as in figure 2b of the same radius R and with height D, its volume is calculated by eq. 5.

$$V_{cyl} = \pi R^2 D \tag{5}$$

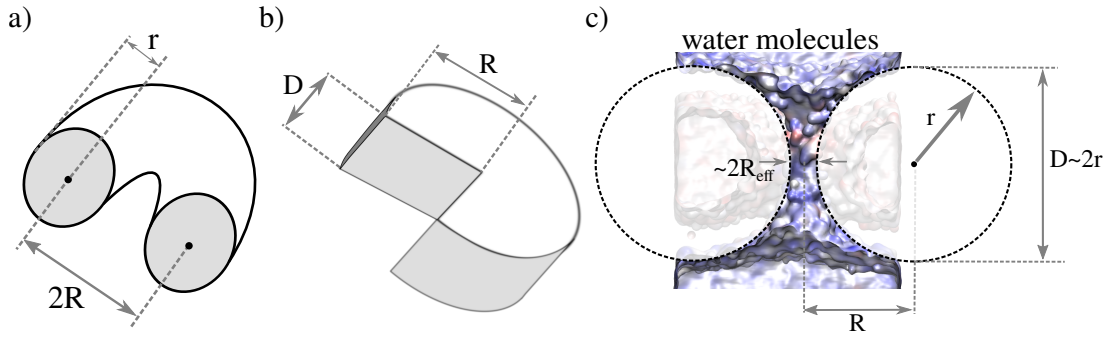

Figure 2: **Volume of the water channel in the expanded fusion pore. a)** Torus. **b)** Cylinder. **c)** Cross-sectional superposition with the toroid-shaped expanded fusion pore. Only water molecules are shown.

The difference between V_{cyl} and the inner-half volume of the torus V_{inner}, is then the volume of the water channel of the expanded fusion pore, see figure 2c. Assuming $D \sim 2r$ and defining $R_{eff} = R - r$ as the radius at the neck of the water channel (see figure 2c), the volume of interest V_{int} is then defined by:

$$V_{int} = V_{cyl} - V_{inner} = \pi D R_{eff}^2 + (\pi - \frac{\pi^2}{4}) D^2 R_{eff} + (\frac{5\pi}{12} - \frac{\pi^2}{8}) D^3 \tag{6}$$

If the effective volume of the toroid-shaped water channel is equal to the volume of an equivalent cylinder of $V_{int} = \pi R_{eq}^2 D$, eq. 6 gives the solution for R_{eff} in the form of a quadratic equation (for more details, see supporting information):

$$R_{eff}^2 + (1 - \frac{\pi}{4}) D R_{eff} + (\frac{5}{12} - \frac{\pi}{8}) D^2 - R_{eq}^2 = 0 \tag{7}$$

Finally, the relation with the collective variable is given by:

$$R_{eq} = R(r)/\sqrt{0.634} + r_0 = (\xi_e + 1) R_0/\sqrt{0.634} + r_0 \tag{8}$$

which includes the 0.634 random close packing correction[49] and the constant $r_0 = 0.5$nm to map $\xi_e \sim 0$ to $R_{eff} \sim 0.2$nm for the just nucleated fusion pore. Therefore, negative values of ξ_e indicate fusion pores with $R_{eff} < 0.2$nm.

Practically, D and R_0 are defined as input parameters for collective variable ξ_e at the beginning of simulations. From the value of ξ_e extracted from molecular dynamics trajectories, eq. 8 gives R_{eq}, which introduced in eq. 7, gives the radius at the neck of the toroid-shaped water channel R_{eff}. Therefore, R_{eff} becomes a convenient measure of the fusion pore dilation. Although almost linear with it (see figure 3d), ξ_e is a dimensionless parameter with less intuitive physical meaning.

Although toroidal fusion pores have been commonly assumed in both computational and experimental studies,[50–54] it has been suggested that asymmetrical shapes are also present,[10] especially for large systems. For fusion pores with radii between ∼1nm and ∼4nm, Jackson and collaborators proposed that a toroid could deform into a catenoid-like surface, overestimating the free energy.[9] Using large DOPC bilayers (45x45nm) with an inter-membrane distance of ∼10nm, Yoo et al.[55] showed that the fusion pore exhibits a bowing feature related to the slow relaxation of the lipids in regions far from the fusion pore. This characteristic could, in principle, help to stabilize large fusion pores.

Collective variables ξ_f, ξ_n and ξ_e do not induce a priori the geometry of the fusion pore. The sliced cylinder strategy biases the system to occupy the inner space of the membrane spanning cylinder along the normal to the bilayers, with no restrictions imposed on the XY planes. Using this technique, Hub and collaborators[25,26] showed that small pores in single bilayers were nearly cylindrical, while larger ones (radius $>$ 1.2nm) revealed a nearly ideal toroidal shape. Systems used along this work belong to the category of small ones (17x17nm) with a maximum fusion pore radius $<$ 1nm (see figure 3c) and were modeled as toroidal. However, we do not discard the existence of different fusion pore shapes for larger systems.

The expanded fusion pore is metastable at $R_{eff} \sim 0.5nm$

Starting from a fusion stalk[28] as the initial configuration, we have nucleated a fusion pore using eq. 2. Nucleation uses a cylinder with N_{sn}=45, d_{sn}=0.25nm, R_{cyln}=0.8nm and ζ_f=0.75. The nucleated fusion pore with a narrow traversing water channel defines the initial config-

uration for the expansion profile at $\xi_e \sim 0$. Fig. 3a shows Potential of Mean Force (PMF) calculations for the expansion of the fusion pore in both directions of collective variable ξ_e: (i) forward (expanding pore, black line) and (ii) backward (shrinking pore, red line).

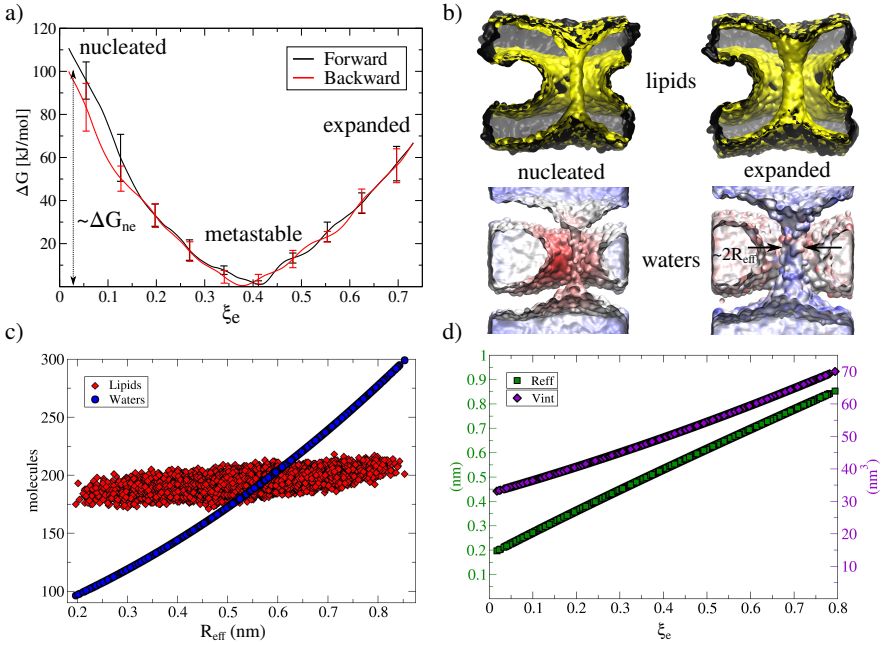

Figure 3: **Sampling and mapping in the ξ_e space. a)** PMF for membranes-only along forward and backward directions. Error bars are standard errors calculated by individually splitting the profiles in independent blocks. **b)** Molecular dynamics snapshots. Nucleated fusion pore for $\xi_e \sim 0$ (left) and expanded fusion pore $\xi_e \sim 0.75$ (right). Lipid molecules are gray with PO4 beads in yellow (top) while water molecules are radially colored in blue and red (bottom). **c)** Mapping the fusion pore effective radius R_{eff} to the amount of water molecules in the channel (blue circles) and to the amount of lipids surrounding it (red diamonds). **d)** Mapping of ξ_e to the effective radius of the fusion pore R_{eff} (green squares) and to the effective volume of the toroid-shaped water channel (purple diamonds).

To expand the fusion pore we have used a slab of height $D = 7nm$ parallel to the bilayers, located at Z_l and with R_{max}=2.5nm (see figure 1e). Normalization radius was set to $R_0 = 0.57$nm. Fusion pore expansion ranges in the interval $0 < \xi_e < 0.75$, see initial and final configurations in figure 3b.

As observed, the free energy profile in figure 3a has a metastable minimum in the interval $0.38 < \xi_e < 0.41$ ($R_{eff} \sim 0.5nm$). By conducting tens of short unbiased molecular dynamics of $\sim$ 250ns (adding a total of $\sim 18\mu$s) from uniformly distributed initial configurations along

ξ_e in the interval [0 0.75], we have measured the amounts of lipids surrounding the water channel and water molecules inside it, see figure 3c. Also, using eqs. 7 and 6, we have used this data to map ξ_e to the effective radius R_{eff} and to the volume V_{int} of the toroid-shaped water channel that defines the fusion pore, see figure 3d. From panel 3d it results that ξ_e is a good measure of the effective radius R_{eff} at the neck of the toroid-shaped expanded fusion pore. The largest fusion pore studied here has an effective radius $R_{eff} \sim 0.85nm$ (see figure 3d).

By definition, ξ_e is an exclusive function of the intra-organelle water molecules and although outnumbered, lipid phosphate heads (PO4). Therefore, the expansion of the fusion pore has a clear effect on the amount of W molecules in the channel, which triples in the interval $0.2 < R_{eff} < 0.85$, see blue circles in figure 3c. The quadratic relation between R_{eff} and the amount of water molecules inside the channel $\sim n_p(r)$, is a result of eqs. 3, 7 and 8, giving $n_p(r) = {R_0}^2(1+\xi_e)^2\pi\frac{D}{v0}$ and considering that ξ_e and R_{eff} are almost directly proportional in the interval $0.2 < \xi_e < 0.8$ (see figure 3e). On the contrary, the amount of lipids surrounding the channel shows little variations, being almost constant around ∼190 molecules, see red squares in figure 3c.

For membranes-only system we report here a decrease of ∼100 kJ/mol ($\sim 40 k_B T$) to drive a just nucleated fusion pore of radius ∼0.2nm to a metastable state of radius ∼0.5nm. Also, we have measured that ∼60 kJ/mol ($\sim 24 k_B T$) are needed to effectively increase the fusion pore radius from 0.5nm to 0.8nm (see figure 3a). In the following sections, we show that the introduction of one or two Syt1-C2B domains in the cytosolic space significantly equalize these energetic barriers, ultimately conditioning the kinetics of the fusion pore.

Hysteresis-free sampling

Theoretically, the free energy cost to evolve from different thermodynamics states (i.e., fused bilayers, nucleation or expansion) must be independent of the direction of the collective variable.[56] Therefore, the opening and closing paths of the fusion pore must be identical in

the free energy profile. Any significant differences between them suggest hysteresis problems, inadequate sampling and/or poor convergence.[57]

To check for hysteresis-free sampling, initial configurations in both directions in the space of ξ_e (forward and backward) were taken from a slow-growth path, as originally suggested by Pearlman and Kollman.[58] Profiles in figure 3a show no significant hysteresis.

The three stages in the life of the fusion pore

The application of ξ_e to the fusion pore completes the free energy landscape together with ξ_f[19,28] and ξ_n.[24,25] As demonstrated before,[19,24–26,28] these collective variables show negligible hysteresis and allow for effective free energy calculations using restrained molecular dynamics simulations. Figure 4 shows schematically the full profile along the life of the fusion pore, from initially flat and parallel bilayers until expansion. The fusion stalk region (lilac) corresponds to our previous study on membrane fusion[28] using collective variable ξ_f. Fusion pore nucleation (pink) was also described previously.[24] A gap in the transition from nucleation to expansion still exists and is indicated in the PMF by a dashed line in the pink region. Fusion pore expansion is colored green and is described in this study using collective variable ξ_e. Expansion beyond $R_{eff} \sim 0.8$nm (marked by the dashed line in the gray region) can be directly obtained using collective variable ξ_e, however, larger R_{eff} may require larger membrane patches to avoid finite size effects.

As shown before,[28] the energy barrier for the first stalk is ΔG_s ~150 kJ/mol for an identical pair of POPC:POPS:PIP_2 bilayers (87.5:10:2.5) in the Martini 3 space, using SAP2 model[32] for PIP_2 lipids. The energy barrier ΔG_n ~350 kJ/mol was also calculated before,[24] for a similar pair of POPC:POPS:PIP_2 bilayers (87.5:10:2.5) in the Martini 2 space using POP2 model for PIP_2 lipids. Stabilization and expansion of the nucleated fusion pore were calculated in this work using Martini 3 for a pair of POPC:POPS:PIP_2 bilayers (87.5:10:2.5) in the Martini 3 space, using also SAP2 model[32] for PIP_2 lipids.

Configurations around a just nucleated fusion pore are difficult to sample. Nucleated

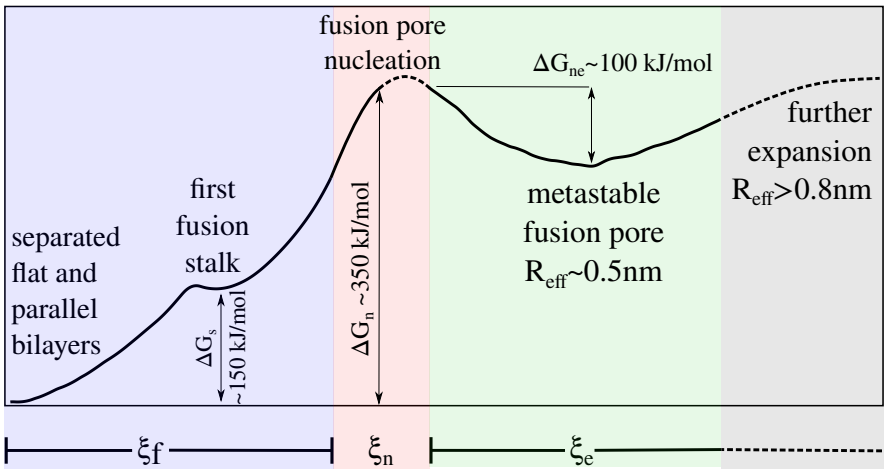

Figure 4: **The life of the fusion pore.** Schematic PMF for stalk formation, fusion pore meta-stabilization and expansion. Solid lines are effective PMF calculations from umbrella sampling simulations, while regions not completely described yet are indicated with dashed lines. In all cases, data corresponds to membranes-only POPC:POPS:PIP_2 systems.

pores easily fall in the expansion region (to the right in figure 4, colored in green) or reseal returning to the stalk (to the left, in figure 4, colored in lilac). Previously, we have studied the nucleation of the fusion pore with negligible hysteresis[24] (represented by the solid line in the pink zone of figure 4). However, a slight widening of the water channel produce unstable configurations that cannot be sustained over long simulation times (dashed line in the pink zone in figure 4). Such behavior prevents adequate sampling in the nucleation region and discourages all attempts to calculate the free energy profile, further in the space of ξ_n. Therefore, once we generated a nucleated fusion pore in the space of ξ_n we have let it evolve freely in the space of ξ_e where it could be later controlled, either to be shrunk or enlarged. The general shape of the schematic PMF shown in figure 4 is in good agreement with other proposed energy landscapes.[20,59–64]

The Synaptotagmin-1 C2B domains reduce the free energy for fusion pore expansion

The presence of a single Syt1-C2B domain in the cytosolic space while membranes fuse and the fusion pore nucleates has shown negligible effects on the free energy profile.[24] However, the simultaneous action of a pair of Syt1-C2B domains (or the tandem Syt1-C2AB) significantly reduced the free energy cost to form the fusion stalk.[28] Here, we complete the scene by describing the C2B domain effects beyond nucleation and during the expansion of the fusion pore. Figure 5 shows free energy profiles in the ξ_e space starting from a nucleated pore ($\xi_e \sim 0$) to an expanded one ($\xi_e \sim 0.75$) for three cases: (i) membranes-only (black line), (ii) with a single Syt1-C2B domain in the cytosolic space (red line) and (iii) with a pair of Syt1-C2B domains also in the cytosolic space (blue line).

From the expanded fusion pore at metastable equilibrium ($\xi_e \sim 0.4$) it is observed that the cost to further expand it to its maximum radius at $\xi_e \sim 0.75$ is reduced by one and two Syt1-C2B domains by $\sim 20 kJ/mol$ each, taking the membranes-only system as reference (black line). Therefore, in agreement with experimental observations,[8,65–67] the presence of Syt1-C2B domains facilitates the metastable fusion pore to evolve towards expansion.

Experimentally, it has been proposed that C2B domains cooperate with the SNARE complexes in bringing the two membranes together.[68,69] Analogously to what has been observed for the fusion stalk,[28] the expansion of the fusion pore is also facilitated by a cooperation mechanism between Syt1-C2B domains. With selected mutations identified in previous experimental studies,[70–72] such cooperative mechanism has been recently verified.[28] These findings point to the relevance of PIP_2 strong anionic interactions with the polybasic patch in Syt1-C2B domains (KRLKKKKTTIKK, positions 321-332), in processes requiring high lipid remodeling, such as membrane bending,[33,67,73,74] membrane fusion[74–77] and the energetically costliest fusion pore expansion.[51,65,78,79]

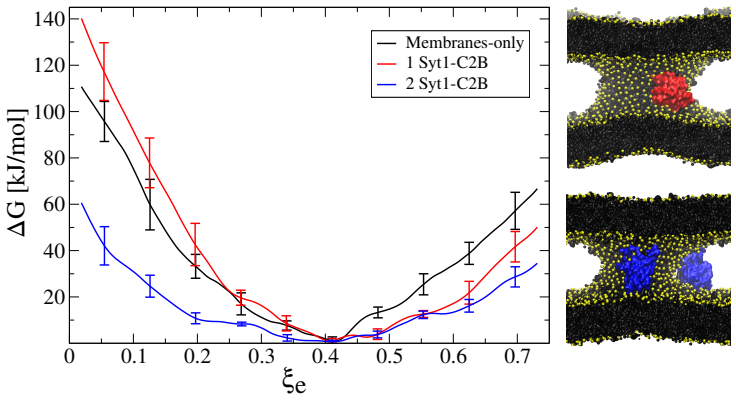

Figure 5: **Free energy profiles for fusion pore expansion.** Membranes-only (black line), with 1 Syt1-C2B domain (red line) and with 2 Syt1-C2B domains (blue line). Error bars are standard errors calculated by individually splitting the profiles in independent blocks. Molecular dynamics snapshots show the expanded pore with one (red) and two (blue) Syt1-C2B domains. Lipid molecules are black with PO4 heads in yellow. For clarity, water molecules are not shown.

Synaptotagmin-1 C2B domains reduce kiss-and-run events

A crucial problem in neurotransmitter release is how the fusion pore regulates the amount of cargo released during exocytosis.[80] Vesicles can either merge with the plasma membrane (full vesicle fusion) or they can release part of their neurotransmitters during transient contacts (kiss-and-run events).[81] From a lipocentric point of view, after the first aqueous connection, fusion pores have been observed to either close or expand towards a metastable state.[12,82] Once there, the metastable fusion pore may continue to expand or it may reseal, still allowing the vesicle to partially deliver its contents (kiss-and-run).[81] If resealing, the fusion pore may flicker, opening and shutting multiple times before expanding again or before definitively closing.[83]

Here, for POPC:POPS:PIP_2 bilayers in the Martini 3 coarse-grained space, we report a nucleation-expansion barrier of ΔG_{ne} ~100 kJ/mol (~$40k_BT$), see figs. 3a and 4. The height of such energy barrier determines the metastability of the fusion pore at $\xi_e \sim 0.4$. Lower values of ΔG_{ne} indicate that the metastable fusion pore at $\xi_e \sim 0.4$ may more easily reconfigure back to a nucleated (and hence unstable) pore at $\xi_e \sim 0$. Remarkably, Syt1-

C2B domains have significant effects on this energy barrier, independently of the effects on expansion ($\xi_e > 0.4$) described in the previous section. Red line in figure 5 shows that one C2B domain marginally increases the nucleation-expansion energy barrier (ΔG_{ne}), see region $0 < \xi_e < 0.4$. However, the opposite effect is observed for a pair of C2B domains surrounding the fusion pore. Blue line shows that $\Delta G_{ne} \sim 60 kJ/mol$, a reduction to almost one-half with respect to membranes-only system. Such collaborative behavior between a pair of C2B domains has already been reported for the fusion stalk.[28]

However, C2B domains not only modify the nucleation-expansion barrier ΔG_{ne} but also the unexplored nucleation region (figure 4, dashed line in the pink zone). We have run 1,000 independent 5ns unbiased simulations from the same initial configuration: a nascent fusion pore at $\xi_e \sim 0$. We have conducted this procedure for the three systems: membranes-only system (black), with one Syt1-C2B (red) and with two Syt1-C2B (blue). Figure 6 concentrates 15 μs of data from molecular dynamics for the three systems. Statistically, it can be observed that the membranes-only system shows the lowest values of ξ_e (even $\xi_e < 0$), indicating the existence of trajectories that evolve in the direction of pore closure and membrane recovery (black). On the contrary, both systems including one (red) or two (blue) Syt1-C2B domains show only positive values of ξ_e with all trajectories evolving toward meta-stabilization at $\xi_e \sim 0.4$ (see panels 6a and 6b).

Moreover, the system with 1 Syt1-C2B has the widest water channel (and the highest values of ξ_e) with the lowest amount of surrounding lipids. On the contrary, membranes-only system has the narrowest water channel (though the lowest values of ξ_e) surrounded by the largest amount of lipids (see panels 6c and 6d). Interestingly, the system with 2 Syt1-C2B domains is in between the other two cases. We hypothesize that the ratio between the amounts of water molecules in the channel and lipids surrounding it, is optimized for 2 Syt1-C2B domains to release free energy and to lower the nucleation expansion barrier ΔG_{ne} (see figure 5). Also, we have observed that 2 Syt1-C2B domains increase the amount of PIP_2:PIP_2 interactions with respect to systems with 1 Syt1-C2B domain and membranes-only (for

details, see supporting information). This increased propensity to form PIP_2 clusters has been observed before[24] and is in agreement with other studies pointing to PIP_2 clusters as molecular beacons during vesicle recruitment.[33,84]

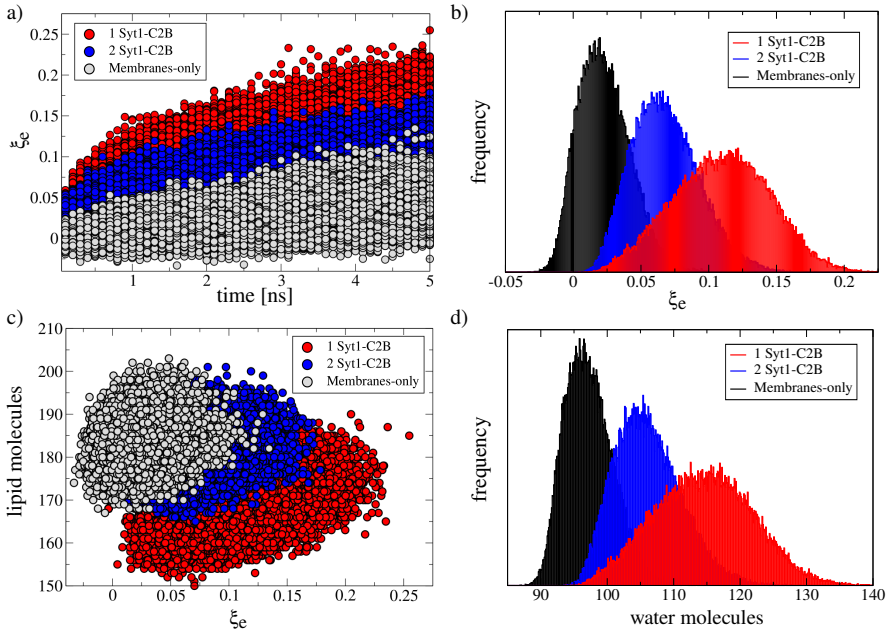

Figure 6: **Unbiased trajectories starting from a nascent just nucleated fusion pore ($\xi_e \sim 0$).** 1,000 simulations per system: membranes-only (black), with 1 Syt1-C2B domain (red) and with 2 Syt1-C2B domains (blue). **a)** Evolution of ξ_e over time. **b)** Histograms of all visited configurations in the space of ξ_e. **c)** Lipid molecules count surrounding the fusion pore channel. **d)** Histograms for intra-organelle water molecules count inside the channel.

Therefore, the presence of one or two Syt1-C2B domains ensures that a nascent fusion pore at $\xi_e \sim 0$ will (most probably) evolve towards meta-stabilization at $\xi_e \sim 0.4$. Once there, the reduced -expansion barrier ΔG_{ne} for two C2B domains facilitates its exit from the metastable state. Together with the reduced cost for expansion ($\xi_e > 0.4$), the system containing a pair of C2B domains naturally evolves in the most probable direction of fusion pore expansion, therefore, significantly reducing the probability of pore resealing and kiss-and-run events.

This effect is also observable for the system containing one C2B domain, which also pushes the nascent fusion pore towards meta-stabilization (see figure 6) and although less significantly, also reduces the cost for expansion for $\xi_e > 0.4$ (see figure 5). However, the

absence of a clear reduction of the nucleation expansion barrier ΔG_{ne} makes the overall effect less noticeable. Accordingly, collaborative mechanisms between pairs of C2B domains (or the tandem C2A:C2B) have already shown to be key during membrane fusion.[28]

In agreement, Cafiso and collaborators[35] hypothesized that Syt1 could mediate the transition during a fusion event by either lowering an energy barrier towards pore expansion (the metastable fusion pore) or by preventing the system from getting trapped at an early intermediate state (a just nucleated fusion pore), as also proposed by Kiessling and collaborators.[85] Moreover, Chapman and collaborators[86] recently observed that the interaction of Syt1 with PIP_2 serves to stabilize opening of fusion pores, while Janshoff and collaborators[87] suggested that Syt1 collaborates to accelerate fusion kinetics in the presence of Ca^{2+}.

On the contrary, the absence of Syt1-C2B domains allow for a just nucleated fusion pore to collapse more easily, letting the system evolve towards pore resealing, and following the path of a kiss-and-run event. This result is in agreement with the hypothesis of flickering fusion pores between lipid membranes in the absence of proteins, proposed more than 20 years ago by Zimmerberg and collaborators.[82] Here, we hypothesize that the Syt1-C2B domains equalize the energy landscape in the nucleation region (figure 4, dashed line in the pink zone) obstructing the path toward the stalk and smoothing it toward the expansion zone.

Conclusions

We have explored the space of fusion pore expansion with the special purpose collective variable ξ_e that drives a just nucleated nascent fusion pore into an expanded configuration. We have studied the effects of one and two Synaptotagmin-1 C2B domains along the expansion of the fusion pore, with the following conclusions: (i) one and two C2B domains in the cytosolic space cumulatively reduce the energetic expansion cost, (ii) one C2B domain marginally increases the nucleation-expansion barrier while two C2B domains significantly reduce it, and (iii) C2B domains systematically push just nucleated nascent fusion pores

toward expansion.

Biological implications of these results are of major importance. First, C2B domains facilitate the expansion of the fusion pore beyond the metastable state at $\xi_e \sim 0.4$ ($R_{eff} \sim 0.5nm$). Second, the nucleation-expansion energy barrier that defines the metastability of the first expanded pore at $\xi_e \sim 0.4$, is significantly reduced by a pair of C2B domains. Combined with the evidence obtained from thousands of independent unbiased simulations, suggesting that a nascent fusion pore (in the nucleation region) has less probability to evolve towards resealing, we have shown that kiss-and-run episodes become less frequent when one or two C2B domains are present. Altogether, these results show that a pair of C2B domains enhance fusion pore expansion and reduce kiss-and-run events.

Our computational predictions could be tested with an experimental setup suitable to study single pore expansion. Accordingly, Khunlo et al.[88] used single vesicle-to-supported bilayer fusion assay to dissect the role of α-synuclein in membrane fusion. Also, Nellikka Rohith et al.[89] used an in vitro approach with v-SNARE–reconstituted nanodiscs and t-SNARE–reconstituted black lipid membrane[86,90] to study α-synuclein modes of action in the micro- and milli-second time-scales. By replacing synuclein by synaptotagmin, these experimental setups could be applied to test our theoretical and computational results.

Computational methods

We have conducted all our simulations using Gromacs-2020.5,[91,92] PLUMED-2.7.2[29] and the Martini 3 coarse-grained model.[30] Molecular dynamics simulations used the semi-isotropic NPT ensemble and a time step of 20fs in all cases. The temperature was set to T=303.15K[93–97] and was controlled by a V-rescale thermostat[98] with a coupling constant of 1ps. The pressure was set at 1.0bar with the compressibility equal to $3\text{x}10^{-4}\text{bar}^{-1}$, using the Parrinello-Rahman barostat[99] with a 12ps time constant. Neighbor search used the Verlet cut-off scheme with a buffer tolerance of 0.005kJ/mol/ps and an update-frequency for the neighbor list equal

to 20 steps. Periodic Boundary Conditions (PBC) were used in all directions. Coulomb interactions used the reaction field method with a cut-off of 1.1nm and a relative dielectric constant of 2.5 (see supporting information for an energy profile using a relative dielectric constant equal to 15). Van der Waals interactions followed the cut-off scheme set to 1.1nm.

In all cases, we have used a pair of lipid bilayers containing 1024 molecules each. These bilayer patches of ∼17x17nm ensure negligible finite-size effects due to interactions between periodic images of the fusion pore.[24,100] The pair of bilayers were solvated in more than ∼30x10^3 W coarse-grained water molecules to fulfill the ample water condition for Martini.[101] The inter-membrane separation was adjusted to equilibrate at ∼3.9nm to fit a Syt1-C2B domain. This inter-membrane distance results in ∼10x10^3 water beads in the cytosolic space.

Figures in this work were created using Visual Molecular Dynamics (VMD),[102] Grace (GRaphing, Advanced Computation and Exploration of data),[103] Inkscape.[104]

PLUMED implementation

We implemented the collective variables to nucleate and expand a fusion pore as two modular C++ files for PLUMED, now available by simply installing the development version of PLUMED 2 (https://github.com/plumed/plumed2) with the membranefusion module enabled (using the keyword -enable-modules=membranefusion). Input/output files and examples are freely available on GitHub: https://github.com/lautarodibartolo/FusionPore. Also, see supporting information for PLUMED example input files.

PMF calculations

Free energy profiles were computed with umbrella sampling[105,106] and recovered with using the Weighted Histogram Analysis Method (WHAM) using the implementation developed by Prof. Grossfield.[107] See supporting information for technical details on windows distribution and convergence analyses.

Acknowledgement

Supercomputing time for this work was provided by CCAD (Centro de Computación de Alto Desempeño de la Universidad Nacional de Córdoba). Grants from CONICET (PIP-0409CO) and ANPCyT (PICT2017-1002) are gratefully acknowledged as well as GPU hardware granted by the NVIDIA Corporation. The authors thank Prof. Jochen Hub for generously sharing his GROMACS source code with us, Prof. Nicolás Wolovick for his help in the parallelization of the ported code and Prof. Giovanni Bussi for his useful advice in PLUMED C++ coding.

Supporting Information Available

Supporting information includes: umbrella sampling technical details and convergence analyses; mathematical details for the calculation of the volume in the toroid-shaped fusion pore; input files for PLUMED to conduct restrained molecular dynamics using collective variable ξ_e.

References

(1) Rizo, J. Molecular Mechanisms Underlying Neurotransmitter Release. *Annu. Rev. Biophys.* **2022**, *51*.

(2) Cohen, R.; Mukai, C.; Nelson, J. L.; Zenilman, S. S.; Sosnicki, D. M.; Travis, A. J. A genetically targeted sensor reveals spatial and temporal dynamics of acrosomal calcium and sperm acrosome exocytosis. *Journal of Biological Chemistry* **2022**, *298*, 101868.

(3) Romarowski, A.; Velasco Félix, A. G.; Torres Rodríguez, P.; Gervasi, M. G.; Xu, X.; Luque, G. M.; Contreras-Jiménez, G.; Sánchez-Cárdenas, C.; Ramírez-Gómez, H. V.; Krapf, D.; Visconti, P. E.; Krapf, D.; Guerrero, A.; Darszon, A.; Buffone, M. G. Super-

resolution imaging of live sperm reveals dynamic changes of the actin cytoskeleton during acrosomal exocytosis. *Journal of cell science* **2018**, *131*, jcs218958.

(4) Tomes, C. The proteins of exocytosis: lessons from the sperm model. *Biochem J* **2015**, *465*, 359–370.

(5) Quevedo, M. F.; Lucchesi, O.; Bustos, M. A.; Pocognoni, C. A.; Paola, X.; Tomes, C. N. The Rab3A-22A chimera prevents sperm exocytosis by stabilizing open fusion pores. *Journal of Biological Chemistry* **2016**, *291*, 23101–23111.

(6) Ruete, M. C.; Lucchesi, O.; Bustos, M. A.; Tomes, C. N. Epac, Rap and Rab3 act in concert to mobilize calcium from sperm's acrosome during exocytosis. *Cell Communication and Signaling* **2014**, *12*, 43.

(7) Buffone, M. G.; Foster, J. A.; Gerton, G. L. The role of the acrosomal matrix in fertilization. *International Journal of Developmental Biology* **2004**, *52*, 511–522.

(8) Wu, Z.; Dharan, N.; McDargh, Z. A.; Thiyagarajan, S.; O'Shaughnessy, B.; Karatekin, E. The neuronal calcium sensor Synaptotagmin-1 and SNARE proteins cooperate to dilate fusion pores. *eLife* **2021**, *10*, e68215.

(9) Chang, C.-W.; Chiang, C.-W.; Jackson, M. B. Fusion pores and their control of neurotransmitter and hormone release. *The Journal of General Physiology* **2017**, *149*, 301–322.

(10) Risselada, H. J.; Grubmüller, H. How proteins open fusion pores: insights from molecular simulations. *European Biophysics Journal* **2021**, *50*, 279–293.

(11) Risselada, H. J.; Mayer, A. SNAREs, tethers and SM proteins: how to overcome the final barriers to membrane fusion? *Biochem J* **2020**, *477*, 243–258.

(12) Risselada, H.; Smirnova, Y.; Grubmüller, H. Free Energy Landscape of Rim-Pore Expansion in Membrane Fusion. *Biophysical Journal* **2014**, *107*, 2287–2295.

(13) Risselada, H. J.; Bubnis, G.; Grubmuller, H. Expansion of the fusion stalk and its implication for biological membrane fusion. *Proc Natl Acad Sci USA* **2014**, *111*, 11043.

(14) Karatekin, E. Toward a unified picture of the exocytotic fusion pore. *FEBS letters* **2018**, *592*, 3563–3585.

(15) Fuertes, G.; Giménez, D.; Esteban-Martín, S.; Sánchez-Muñoz, O. L.; Salgado, J. A lipocentric view of peptide-induced pores. *European biophysics journal : EBJ* **2011**, *40*, 399–415.

(16) Cunill-Semanat, E.; Salgado, J. Spontaneous and Stress-Induced Pore Formation in Membranes: Theory, Experiments and Simulations. *The Journal of Membrane Biology* **2019**, *252*, 241–260.

(17) Aeffner, S.; Reusch, T.; Weinhausen, B.; Salditt, T. Energetics of stalk intermediates in membrane fusion are controlled by lipid composition. *Proc Natl Acad Sci USA* **2012**, *109*, E1609.

(18) Smirnova, Y. G.; Risselada, H. J.; Müller, M. Thermodynamically reversible paths of the first fusion intermediate reveal an important role for membrane anchors of fusion proteins. *Proceedings of the National Academy of Sciences* **2019**, *116*, 2571–2576.

(19) Poojari, C. S.; Scherer, K. C.; Hub, J. S. Free energies of membrane stalk formation from a lipidomics perspective. *Nature Communications* **2021**, *12*, 6594.

(20) Smirnova, Y. G.; Fuhrmans, M.; Vidal, I. A. B.; Müller, M. Free-energy calculation methods for collective phenomena in membranes. *Journal of Physics D* **2015**, *48*, 343001.

(21) Kawamoto, S.; Shinoda, W. Free energy analysis along the stalk mechanism of membrane fusion. *Soft Matter* **2014**, *10*, 3048–3054.

(22) Shinoda, W.; DeVane, R.; Klein, M. L. Zwitterionic Lipid Assemblies: Molecular Dynamics Studies of Monolayers, Bilayers, and Vesicles Using a New Coarse Grain Force Field. *J. Phys. Chem. B* **2010**, *114*, 6836–6849.

(23) Kawamoto, S.; Klein, M. L.; Shinoda, W. Coarse-grained molecular dynamics study of membrane fusion: Curvature effects on free energy barriers along the stalk mechanism. *J. Chem. Phys.* **2015**, *143*, 243112.

(24) Caparotta, M.; Tomes, C. N.; Mayorga, L. S.; Masone, D. The Synaptotagmin-1 C2B Domain Is a Key Regulator in the Stabilization of the Fusion Pore. *J. Chem. Theory Comput.* **2020**, *16*, 7840–7851.

(25) Hub, J. S.; Awasthi, N. Probing a Continuous Polar Defect: A Reaction Coordinate for Pore Formation in Lipid Membranes. *J. Chem. Theory Comput.* **2017**, *13*, 2352–2366.

(26) Hub, J. S. Joint Reaction Coordinate for Computing the Free-Energy Landscape of Pore Nucleation and Pore Expansion in Lipid Membranes. *J. Chem. Theory Comput.* **2021**, *17*, 1229–1239.

(27) Fernandez, I.; Arac, D.; Ubach, J.; Gerber, S. H.; Shin, O.-h.; Gao, Y.; Anderson, R. G. W.; Sudhof, T. C.; Rizo, J. Three-Dimensional Structure of the Synaptotagmin 1 C2B-Domain: Synaptotagmin 1 as a Phospholipid Binding Machine. *Neuron* **2001**, *32*, 1057–1069.

(28) Di Bartolo, A. L.; Masone, D. Synaptotagmin-1 C2B domains cooperatively stabilize the fusion stalk via a master-servant mechanism. *Chem. Sci.* **2022**, *13*, 3437–3446.

(29) Tribello, G.; Bonomi, M.; Branduardi, D.; Camilloni, C.; Bussi, G. PLUMED 2: New feathers for an old bird. *Computer Physics Communications* **2014**, *185*, 604–613.

(30) Souza, P. C. T.; Alessandri, R.; Barnoud, J.; Thallmair, S.; Faustino, I.; Grünewald, F.; Patmanidis, I.; Abdizadeh, H.; Bruininks, B. M. H.; Wassenaar, T. A.; Kroon, P. C.;

Melcr, J.; Nieto, V.; Corradi, V.; Khan, H. M.; Domański, J.; Javanainen, M.; Martinez-Seara, H.; Reuter, N.; Best, R. B.; Vattulainen, I.; Monticelli, L.; Periole, X.; Tieleman, D. P.; de Vries, A. H.; Marrink, S. J. Martini 3: a general purpose force field for coarse-grained molecular dynamics. *Nature Methods* **2021**, *18*, 382–388.

(31) Perez-Lara, A.; Thapa, A.; Nyenhuis, S. B.; Nyenhuis, D. A.; Halder, P.; Tietzel, M.; Tittmann, K.; Cafiso, D. S.; Jahn, R. PtdInsP(2) and PtdSer cooperate to trap synaptotagmin-1 to the plasma membrane in the presence of calcium. *eLife* **2016**, *5*, e15886.

(32) Borges-Araújo, L.; Souza, P. C. T.; Fernandes, F.; Melo, M. N. Improved Parameterization of Phosphatidylinositide Lipid Headgroups for the Martini 3 Coarse-Grain Force Field. *J. Chem. Theory Comput.* **2022**, *18*, 357–373.

(33) Honigmann, A.; van den Bogaart, G.; Iraheta, E.; Risselada, H. J.; Milovanovic, D.; Mueller, V.; Mullar, S.; Diederichsen, U.; Fasshauer, D.; Grubmuller, H.; Hell, S. W.; Eggeling, C.; Kuhnel, K.; Jahn, R. Phosphatidylinositol 4,5-bisphosphate clusters act as molecular beacons for vesicle recruitment. *Nature structural & molecular biology* **2013**, *20*, 679–686.

(34) Wu, Z.; Ma, L.; Zhu, J.; Courtney, N.; Zhang, Y.; Chapman, E. R.; Karatekin, E. A Polybasic Patch on Synaptotagmin-1 C2A Domain is Essential for Evoked Release and Dilation of Fusion Pores. *Biophysical Journal* **2020**, *118*, 400a.

(35) Nyenhuis, S. B.; Karandikar, N.; Kiessling, V.; Kreutzberger, A. J. B.; Thapa, A.; Liang, B.; Tamm, L. K.; Cafiso, D. S. Conserved arginine residues in synaptotagmin 1 regulate fusion pore expansion through membrane contact. *Nature Communications* **2021**, *12*, 761.

(36) Bai, J.; Tucker, W. C.; Chapman, E. R. PIP2 increases the speed of response of synap-

totagmin and steers its membrane-penetration activity toward the plasma membrane. *Nature Structural & Molecular Biology* **2004**, *11*, 36–44.

(37) Li, L.; Shin, O.-H.; Rhee, J.-S.; Arac, D.; Rah, J.-C.; Rizo, J.; Sudhof, T.; Rosenmund, C. Phosphatidylinositol Phosphates as Co-activators of Ca2+ Binding to C2 Domains of Synaptotagmin 1. *Journal of Biological Chemistry* **2006**, *281*, 15845–15852.

(38) Radhakrishnan, A.; Stein, A.; Jahn, R.; Fasshauer, D. The Ca2+ affinity of synaptotagmin 1 is markedly increased by a specific interaction of its C2B domain with phosphatidylinositol 4,5-bisphosphate. *The Journal of biological chemistry* **2009**, *284*, 25749–25760.

(39) Kuo, W.; Herrick, D. Z.; Ellena, J. F.; Cafiso, D. S. The calcium-dependent and calcium-independent membrane binding of synaptotagmin 1: two modes of C2B binding. *Journal of molecular biology* **2009**, *387*, 284–294.

(40) van den Bogaart, G.; Thutupalli, S.; Risselada, J. H.; Meyenberg, K.; Holt, M.; Riedel, D.; Diederichsen, U.; Herminghaus, S.; Grubmüller, H.; Jahn, R. Synaptotagmin-1 may be a distance regulator acting upstream of SNARE nucleation. *Nature Structural & Molecular Biology* **2011**, *18*, 805–812.

(41) Klein, F.; Cáceres, D.; Carrasco, M. A.; Tapia, J. C.; Caballero, J.; Alzate-Morales, J.; Pantano, S. Coarse-Grained Parameters for Divalent Cations within the SIRAH Force Field. *J. Chem. Inf. Model.* **2020**, *60*, 3935–3943.

(42) Marrink, S. J.; Tieleman, D. P. Perspective on the Martini model. *Chem. Soc. Rev.* **2013**, *42*, 6801–6822.

(43) Sharma, S.; Lindau, M. Molecular mechanism of fusion pore formation driven by the neuronal SNARE complex. *Proceedings of the National Academy of Sciences* **2018**, *115*, 12751–12756.

(44) Jackson, M. B. Minimum membrane bending energies of fusion pores. *The Journal of membrane biology* **2009**, *231*, 101–115.

(45) Cohen, F. S.; Melikyan, G. B. The Energetics of Membrane Fusion from Binding, through Hemifusion, Pore Formation, and Pore Enlargement. *The Journal of Membrane Biology* **2004**, *199*, 1–14.

(46) Bernal, J.; Mason, J. Packing of spheres: co-ordination of randomly packed spheres. *Nature* **1960**, *188*, 910–911.

(47) Scott, G. D.; Kilgour, D. M. The density of random close packing of spheres. *Journal of Physics D: Applied Physics* **1969**, *2*, 863.

(48) Berryman, J. G. Random close packing of hard spheres and disks. *Physical Review A* **1983**, *27*, 1053.

(49) Song, C.; Wang, P.; Makse, H. A. A phase diagram for jammed matter. *Nature* **2008**, *453*, 629–632.

(50) Kozlov, M. M.; Leikin, S. L.; Chernomordik, L. V.; Markin, V. S.; Chizmadzhev, Y. A. Stalk mechanism of vesicle fusion - Intermixing of aqueous contents. *European Biophysics Journal* **1989**, *17*, 121–129.

(51) Chizmadzhev, Y. A.; Cohen, F. S.; Shcherbakov, A.; Zimmerberg, J. Membrane mechanics can account for fusion pore dilation in stages. *Biophysical Journal* **1995**, *69*, 2489–2500.

(52) Sobko, A. A.; Kotova, E. A.; Antonenko, Y. N.; Zakharov, S. D.; Cramer, W. A. Lipid dependence of the channel properties of a colicin E1-lipid toroidal pore. *Journal of Biological Chemistry* **2006**, *281*, 14408–14416.

(53) Mihajlovic, M.; Lazaridis, T. Antimicrobial peptides in toroidal and cylindrical pores. *Biochimica et Biophysica Acta (BBA)-Biomembranes* **2010**, *1798*, 1485–1493.

(54) Wu, Z.; Bello, O. D.; Thiyagarajan, S.; Auclair, S. M.; Vennekate, W.; Krishnakumar, S. S.; O'Shaughnessy, B.; Karatekin, E. Dilation of fusion pores by crowding of SNARE proteins. *Elife* **2017**, *6*, e22964.

(55) Yoo, J.; Jackson, M. B.; Cui, Q. A comparison of coarse-grained and continuum models for membrane bending in lipid bilayer fusion pores. *Biophysical journal* **2013**, *104*, 841–852.

(56) Neale, C.; Pomes, R. Sampling errors in free energy simulations of small molecules in lipid bilayers. *Biosimulations of lipid membranes coupled to experiments* **2016**, *1858*, 2539–2548.

(57) Awasthi, N.; Hub, J. S. Simulations of Pore Formation in Lipid Membranes: Reaction Coordinates, Convergence, Hysteresis, and Finite-Size Effects. *J. Chem. Theory Comput.* **2016**, *12*, 3261–3269.

(58) Pearlman, D. A.; Kollman, P. A. The lag between the Hamiltonian and the system configuration in free energy perturbation calculations. *J. Chem. Phys.* **1989**, *91*, 7831–7839.

(59) Lipowsky, R. Remodeling of Membrane Shape and Topology by Curvature Elasticity and Membrane Tension. *Adv. Biology* **2022**, *6*, 2101020.

(60) Gorai, B.; Sahoo, A. K.; Srivastava, A.; Dixit, N. M.; Maiti, P. K. Concerted Interactions between Multiple gp41 Trimers and the Target Cell Lipidome May Be Required for HIV-1 Entry. *J. Chem. Inf. Model.* **2021**, *61*, 444–454.

(61) Dhara, M.; Mantero Martinez, M.; Makke, M.; Schwarz, Y.; Mohrmann, R.; Bruns, D. Synergistic actions of v-SNARE transmembrane domains and membrane-curvature modifying lipids in neurotransmitter release. *eLife* **2020**, *9*, e55152.

(62) Claire, F.-M.; Rothman James, E.; Frederic, P. Low energy cost for optimal speed and control of membrane fusion. *Proceedings of the National Academy of Sciences* **2017**, *114*, 1238–1241.

(63) Kawamoto, S.; Shinoda, W. Free energy analysis along the stalk mechanism of membrane fusion. *Soft Matter* **2014**, *10*, 3048–3054.

(64) Markvoort, A. J.; Marrink, S. J. In *Current Topics in Membranes*; Chernomordik, L. V., Kozlov, M. M., Eds.; Academic Press, 2011; Vol. 68; pp 259–294.

(65) Bendahmane, M.; Bohannon, K. P.; Bradberry, M. M.; Rao, T. C.; Schmidtke, M. W.; Abbineni, P. S.; Chon, N. L.; Tran, S.; Lin, H.; Chapman, E. R.; Knight, J. D.; Anantharam, A. The synaptotagmin C2B domain calcium-binding loops modulate the rate of fusion pore expansion. *Molecular biology of the cell* **2018**, *29*, 834–845.

(66) Ying, L.; Jiajie, D.; Yanxin, L.; Yuji, I.; Zengliu, S.; Klaus, S.; Taekjip, H.; Yeon-Kyun, S. Fusion pore formation and expansion induced by Ca2+ and synaptotagmin 1. *Proceedings of the National Academy of Sciences* **2013**, *110*, 1333–1338.

(67) Lynch, K. L.; Gerona, R. R. L.; Kielar, D. M.; Martens, S.; McMahon, H. T.; Martin, T. F. J. Synaptotagmin-1 utilizes membrane bending and SNARE binding to drive fusion pore expansion. *Molecular biology of the cell* **2008**, *19*, 5093–5103.

(68) Wang, S.; Li, Y.; Ma, C. Synaptotagmin-1 C2B domain interacts simultaneously with SNAREs and membranes to promote membrane fusion. *eLife* **2016**, *5*, e14211.

(69) Brewer, K. D.; Bacaj, T.; Cavalli, A.; Camilloni, C.; Swarbrick, J. D.; Liu, J.; Zhou, A.; Zhou, P.; Barlow, N.; Xu, J.; Seven, A. B.; Prinslow, E. A.; Voleti, R.; Häussinger, D.; Bonvin, A. M. J. J.; Tomchick, D. R.; Vendruscolo, M.; Graham, B.; Südhof, T. C.; Rizo, J. Dynamic binding mode of a Synaptotagmin-1-SNARE complex in solution. *Nature Structural & Molecular Biology* **2015**, *22*, 555–564.

(70) Roggero, C. M.; Tomes, C. N.; De Blas, G. A.; Castillo, J.; Michaut, M. A.; Fukuda, M.; Mayorga, L. S. Protein kinase C-mediated phosphorylation of the two polybasic regions of synaptotagmin VI regulates their function in acrosomal exocytosis. *Developmental Biology* **2005**, *285*, 422–435.

(71) Roggero, C. M.; De Blas, G. A.; Dai, H.; Tomes, C. N.; Rizo, J.; Mayorga, L. S. Complexin/Synaptotagmin Interplay Controls Acrosomal Exocytosis. *Journal of Biological Chemistry* **2007**, *282*, 26335–26343.

(72) Gaffaney, J. D.; Dunning, F. M.; Wang, Z.; Hui, E.; Chapman, E. R. Synaptotagmin C2B Domain Regulates Ca²⁺-triggered Fusion in Vitro: CRITICAL RESIDUES REVEALED BY SCANNING ALANINE MUTAGENESIS *. *Journal of Biological Chemistry* **2008**, *283*, 31763–31775.

(73) Shukla, S.; Jin, R.; Robustelli, J.; Zimmerman, Z. E.; Baumgart, T. PIP2 Reshapes Membranes through Asymmetric Desorption. *Biophysical Journal* **2019**, *117*, 962–974.

(74) McMahon, H. T.; Kozlov, M. M.; Martens, S. Membrane Curvature in Synaptic Vesicle Fusion and Beyond. *Cell* **2010**, *140*, 601–605.

(75) Mu, L.; Tu, Z.; Miao, L.; Ruan, H.; Kang, N.; Hei, Y.; Chen, J.; Wei, W.; Gong, F.; Wang, B.; Du, Y.; Ma, G.; Amerein, M. W.; Xia, T.; Shi, Y. A phosphatidylinositol 4,5-bisphosphate redistribution-based sensing mechanism initiates a phagocytosis programing. *Nature Communications* **2018**, *9*, 4259.

(76) Park, Y.; Ryu, J.-K. Models of synaptotagmin-1 to trigger Ca2+-dependent vesicle fusion. *FEBS Lett* **2018**, *592*, 3480–3492.

(77) James, D. J.; Khodthong, C.; Kowalchyk, J. A.; Martin, T. F. J. Phosphatidylinositol 4,5-bisphosphate regulates SNARE-dependent membrane fusion. *J Cell Biol* **2008**, *182*, 355–366.

(78) Ryham, R. J.; Ward, M. A.; Cohen, F. S. Teardrop shapes minimize bending energy of fusion pores connecting planar bilayers. *Phys. Rev. E* **2013**, *88*, 062701.

(79) Nanavati, C.; Markin, V. S.; Oberhauser, A. F.; Fernandez, J. M. The exocytotic fusion pore modeled as a lipidic pore. *Biophysical journal* **1992**, *63*, 1118–1132.

(80) Staal, R. G. W.; Mosharov, E. V.; Sulzer, D. Dopamine neurons release transmitter via a flickering fusion pore. *Nature Neuroscience* **2004**, *7*, 341–346.

(81) Chapman, E. R. How Does Synaptotagmin Trigger Neurotransmitter Release? *Annu. Rev. Biochem.* **2008**, *77*, 615–641.

(82) Chanturiya, A.; Chernomordik, L. V.; Zimmerberg, J. Flickering fusion pores comparable with initial exocytotic pores occur in protein-free phospholipid bilayers. *Proceedings of the National Academy of Sciences* **1997**, *94*, 14423–14428.

(83) Wu, Z.; Thiyagarajan, S.; O'Shaughnessy, B.; Karatekin, E. Regulation of Exocytotic Fusion Pores by SNARE Protein Transmembrane Domains. *Frontiers in Molecular Neuroscience* **2017**, *10*.

(84) van den Bogaart, G.; Meyenberg, K.; Risselada, H. J.; Amin, H.; Willig, K. I.; Hubrich, B. E.; Dier, M.; Hell, S. W.; Grubmüller, H.; Diederichsen, U.; Jahn, R. Membrane protein sequestering by ionic protein-lipid interactions. *Nature* **2011**, *479*, 552–555.

(85) Tamm, L. K.; Crane, J.; Kiessling, V. Membrane fusion: a structural perspective on the interplay of lipids and proteins. *Current opinion in structural biology* **2003**, *13*, 453–466.

(86) Das, D.; Bao, H.; Courtney, K. C.; Wu, L.; Chapman, E. R. Resolving kinetic intermediates during the regulated assembly and disassembly of fusion pores. *Nature Communications* **2020**, *11*, 231.

(87) Dietz, J.; Oelkers, M.; Hubrich, R.; Pérez-Lara, A.; Jahn, R.; Steinem, C.; Janshoff, A. Forces, Kinetics, and Fusion Efficiency Altered by the Full-Length Synaptotagmin-1 -PI(4,5)P2 Interaction in Constrained Geometries. *Nano Lett.* **2022**, *22*, 1449–1455.

(88) Khounlo, R.; Hawk, B. J. D.; Khu, T.-M.; Yoo, G.; Lee, N. K.; Pierson, J.; Shin, Y.-K. Membrane Binding of alpha-Synuclein Stimulates Expansion of SNARE-Dependent Fusion Pore. *Frontiers in cell and developmental biology* **2021**, *9*, 663431–663431.

(89) Nellikka Rohith, K.; Bhaskar Bhavya, R.; Kinjal, S.; Patil Swapnali, S.; Debasis, D. alpha-Synuclein kinetically regulates the nascent fusion pore dynamics. *Proceedings of the National Academy of Sciences* **2021**, *118*, e2021742118.

(90) Bao, H.; Das, D.; Courtney, N. A.; Jiang, Y.; Briguglio, J. S.; Lou, X.; Roston, D.; Cui, Q.; Chanda, B.; Chapman, E. R. Dynamics and number of trans-SNARE complexes determine nascent fusion pore properties. *Nature* **2018**, *554*, 260.

(91) Van Der Spoel, D.; Lindahl, E.; Hess, B.; Groenhof, G.; Mark, A. E.; Berendsen, H. J. C. GROMACS: Fast, flexible, and free. *Journal of Computational Chemistry* **2005**, *26*, 1701–1718.

(92) Abraham, M. J.; Murtola, T.; Schulz, R.; Páll, S.; Smith, J. C.; Hess, B.; Lindahl, E. GROMACS: High performance molecular simulations through multi-level parallelism from laptops to supercomputers. *SoftwareX* **2015**, *1-2*, 19–25.

(93) Caparotta, M.; Bustos, D. M.; Masone, D. Order-disorder skewness in alpha-synuclein: a key mechanism to recognize membrane curvature. *Phys. Chem. Chem. Phys.* **2020**, *22*, 5255–5263.

(94) Masone, D.; Uhart, M.; Bustos, D. M. Bending Lipid Bilayers: A Closed-Form Collective Variable for Effective Free-Energy Landscapes in Quantitative Biology. *J. Chem. Theory Comput.* **2018**, *14*, 2240–2245.

(95) Jo, S.; Lim, J. B.; Klauda, J. B.; Im, W. CHARMM-GUI Membrane Builder for Mixed Bilayers and Its Application to Yeast Membranes. *Biophysical Journal* **2009**, *97*, 50–58.

(96) Rui, H.; Lee, K. I.; Pastor, R. W.; Im, W. Molecular Dynamics Studies of Ion Permeation in VDAC. *Biophysical Journal* **2011**, *100*, 602–610.

(97) Jo, S.; Kim, T.; Im, W. Automated Builder and Database of Protein/Membrane Complexes for Molecular Dynamics Simulations. *PLoS ONE* **2007**, *2*, e880–.

(98) Bussi, G.; Donadio, D.; Parrinello, M. Canonical sampling through velocity rescaling. *The Journal of Chemical Physics* **2007**, *126*, 014101.

(99) Parrinello, M.; Rahman, A. Polymorphic transitions in single crystals: A new molecular dynamics method. *Journal of Applied Physics* **1981**, *52*, 7182–7190.

(100) Caparotta, M.; Puiatti, M.; Masone, D. Artificial stabilization of the fusion pore by intra-organelle styrene–maleic acid copolymers. *Soft Matter* **2021**, *17*, 8314–8321.

(101) Ingolfsson, H. I.; Melo, M. N.; van Eerden, F. J.; Arnarez, C.; Lopez, C. A.; Wassenaar, T. A.; Periole, X.; de Vries, A. H.; Tieleman, D. P.; Marrink, S. J. Lipid Organization of the Plasma Membrane. *J. Am. Chem. Soc.* **2014**, *136*, 14554–14559.

(102) Humphrey, W.; Dalke, A.; Schulten, K. VMD - Visual Molecular Dynamics. *Journal of Molecular Graphics* **1996**, *14*, 33–38.

(103) Grace Development Team, GRACE: GRaphing, Advanced Computation and Exploration of data. `https://plasma-gate.weizmann.ac.il/Grace/`, Last accessed: Jun 2022.

(104) Inkscape Project, Inkscape. `https://inkscape.org`, Last accessed: Jun 2022.

(105) Torrie, G.; Valleau, J. Nonphysical sampling distributions in Monte Carlo free-energy estimation: Umbrella sampling. *Journal of Computational Physics* **1977**, *23*, 187–199.

(106) Roux, B. The calculation of the potential of mean force using computer simulations. *Comput. Phys. Commun.* **1995**, *91*, 275–282.

(107) Grossfield, A. WHAM: the weighted histogram analysis method. `http://membrane.urmc.rochester.edu/wordpress/?page_id=126`, version 2.0.9.1; Last accessed: Jun 2022.

Graphical TOC Entry